Soft Magnetic-Actuation-Based Haptic Interface for a Robot-Assisted Vascular Interventional System: A Feasibility Study

Xinming Li, *Graduate Student Member, IEEE*, Shuxiang Guo, *Fellow, IEEE*, Keisuke Suzuki, Peng Shi, *Member, IEEE*, and Xiaoliang Jin, *Member, IEEE*

***Abstract*—As a promising alternative for minimally invasive vascular surgery, robot-assisted vascular interventional system (VIS) has expressed considerable benefits in preventing radiation, decreasing workload for surgeons, improving surgical environment, and reducing postoperative risk for patients. However, the existing robotic VISs ignore to employ proper haptic feedback for robot-assisted surgery owing to the short of flexible and controllable capabilities of haptic perception. In this work, we develop a dual-instrument operating robotic VIS to manipulate guidewire and catheter, which is capable for multi-instrument surgical tasks. Most importantly, a soft magnetic-actuation-based haptic interface, a prospective solution for haptic sensing based on flexible combination of soft material and magnetic material, is proposed to provide adjustable haptic information for operators. Moreover, a safety operation strategy based on the proposed haptic interface is designed to ensure a safer operating environment for interaction between master side and slave side. Four kinds of experiments are performed to demonstrate the feasibility of soft magnetic-actuation-based haptic feedback and evaluate the tracking performance and operating performance of developed robot-assisted VIS. Results prove the engineering feasibility (haptic sensing range: 0.01–1.49 N) of the proposed haptic interface and the operating effectiveness of developed robot-assisted VIS (maximum linear error is 1.87 mm). Besides, this effort probably has a potential impact on the implementation of soft haptic feedback, research of multi-instrument device, and improvement of safety operation for robotic systems.**

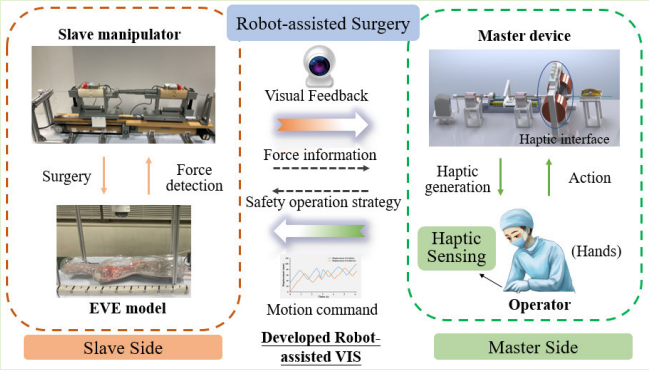

***Index Terms*—Haptic sensing, robot-assisted vascular interventional system (VIS), safety operation strategy, soft magnetic-actuation-based haptic interface.**

Manuscript received 9 October 2023; revised 6 November 2023; accepted 7 November 2023. Date of publication 16 November 2023; date of current version 2 January 2024. This work was supported in part by the Japan Society for the Promotion of Science (SPS) KAKENHI under Grant 15K2120 and in part by the National High-Tech Research and Development Program (863 Program) of China under Grant 2015AA043202. The associate editor coordinating the review of this article and approving it for publication was Prof. Dongsoo Har. *(Corresponding authors: Shuxiang Guo; Keisuke Suzuki.)*

Xinming Li, Keisuke Suzuki, Peng Shi, and Xiaoliang Jin are with the Graduate School of Engineering, Kagawa University, Takamatsu 761-0396, Japan (e-mail: s21d504@kagawa-u.ac.jp; suzuki.keisuke@kagawa-u.ac.jp; s19d503@stu.kagawa-u.ac.jp; s19d505@stu.kagawa-u.ac.jp).

Shuxiang Guo is with the Department of Electronic and Electrical Engineering, Southern University of Science and Technology, Shenzhen 518055, China, and also with the School of Life Science and the Key Laboratory of Convergence Medical Engineering System and Healthcare Technology, Ministry of Industry and Information Technology, Beijing Institute of Technology, Beijing 100081, China (e-mail: guo.shuxiang@sustech.edu.cn).

Digital Object Identifier 10.1109/JSEN.2023.3332041

I. Introduction

ROBOT-ASSISTED vascular interventional system (VIS) has embraced growing interest and attention for the field of minimally invasive vascular surgery on account of advantages for the protection of X-ray radiation and reduction of orthopedic strain injuries for physicians [1]. Concurrently, robot-assisted VIS also has potential benefits over vascular surgery, few postoperative complications, and quick recovery for patients with cardiovascular disease. Unlike conventional minimally invasive vascular surgery, the robot-assisted VIS enables physician to provide insert-extract motion and rotation motion of catheter/guidewire by the master device placed in a separate location [2]. Accordingly, the slave manipulator mounted on the operating room controls surgical instruments to conduct robot-assisted surgery. Hence, the design of master–slave [3], [4], [5] makes it possible to complete remote surgery in medically underserved regions, especially under

the current epidemic-ridden environment. Generally, robot-assisted system relies on faster and more accurate interaction among robotic system, patient, and surgeon. Moreover, flexible and precise haptic perception is significant for force interaction between the master side (operation side for physician) and the slave side (surgical side for patient) [6], which is able to improve transparency and safety of surgical procedure via offering a real sensation of surgical resistance for operators.

The relevant efforts for robot-assisted VIS mainly focused on the designs of master–slave assistance [7], [8] and implementations of the sense of haptic feedback [9], [10]. For the area of master–slave assistance, a large number of robots have been proposed to complete robot-assisted surgery. Yang et al. [11] proposed a master–slave interventional surgical robot based on an isomorphic interactive device, which has ability to perform complex operations in remote surgery. However, it occupies a large volume space for compact design. Bao et al. [12] designed a telerobotic system based on two commercial haptic devices (TouchTM X, USA). This robotic system was validated through both laboratory experiments and in-human experiments without considering surgeon's natural surgical skills [13]. Kundrat et al. [14] designed an endovascular robotic platform, which offered inspiration for clinical translation with device deployment using MR-safe teleoperation platform, but the master device is designed for only one instrument. Wang et al. [15] presented a 12-degrees of freedom (DOFs) insertion system with a higher redundancy to achieve the movement of surgical instruments. Chen et al. [16] proposed a magnetic micro active guidewire for surgical application to reduce operating time, whereas it was pretty tough to insert into the vessels with complex shapes limited by the size. Above all, these works mainly dedicate to use rocker devices (commercial or self-designed) or single instrument control, and a few studies focus on multi-instrument manipulation and natural operating habits of surgeons for master–slave system. Hence, a novel VIS using coaxial operation for natural operation and multi-instrument control is developed in this effort.

For the related studies [9], [10] of haptic feedback, researchers mainly focus on building more realistic haptic sensing on the master side to improve the surgical immersion. For example, a highly sensitive visual force senor with small size [17] was designed to collect force signal, which can offer more intuitive force feedback. However, it is still limited due to the lack of effective robot-assisted validation. Zhou et al. [18] designed a surgeon's habits-based master manipulator as a single operating unit with both axial and circumferential haptic feedback on master side, which is helpful for tactile implementation of robot-assisted VIS, but the operating handle is truly different from the real medical instrument. Besides, a master device [19] was proposed to offer a good sense of haptic resistance via the magnetorheological (MR) fluids with the inevitable limitation of the physical properties that fluids are difficult to control. Linear motor was employed to generate haptic feedback [20], which can build integrated haptic feedback. However, it needs extra energy to overcome the internal resistance of motor. Above all, these efforts pay attention to achieve the haptic feedback via designed sensors or special mechanical structure. Consequently, a lightweight soft solution based on magnetic-actuation-based haptic interface was designed to provide flexible, controllable, and reusable haptic feedback in this work.

Based on the above efforts, the study for robot-assisted VIS is still challenging for multi-instrument control between master–slave side and flexible design for accurate, controllable, and repeatable haptic feedback. In this work, we mainly work on the achievements of VIS, haptic sensing (generated by haptic interface), and safety operation. The key contributions are summarized as follows.

1) A robot-assisted VIS with two operating units was developed to conduct the surgery, which has ability to control two kinds of surgical instruments (catheter and guidewire) simultaneously for actual operation.
2) A soft magnetic-actuation-based haptic interface was conceived and designed to generate a sensing of haptic based on soft magnetic-actuation-based structure (SMAS) (detected haptic sensing range: 0.01–1.49 N), which is a bold attempt for exploring the possibility of combination of soft material and magnetic material to provide haptic feedback for robotic systems (a green and compatible solution).
3) A safety operation strategy was proposed to guarantee a safer robot-assisted surgical environment via changing the sensing of haptic feedback for operators and controlling the movement of robotic manipulator for patient. Hence, this strategy can ensure a safer operating situation for both operator and patient.

Considering these contributions, this work has potential values for inspirating and motivating further research in relevant fields, including robot-assisted surgery for multi-instrument, flexible and controllable solution for haptic sensing, and safety operation for master–slave robotic system.

The remainder of this effort is organized as follows. Section II describes the developed robot-assisted VIS based on a remote design of master–slave structure. Section III is the details of the proposed haptic interface and safety operation strategy. Experiments and results are exhibited in Section IV. Section V organizes the discussion part of this work. At the end, Section VI presents the conclusion.

II. Developed Vascular Interventional System

The developed robot-assisted VIS is a teleoperation robotic system. Fig. 1 depicts the conceptual diagram of the developed robot-assisted VIS. Master device locates in a control room (master side), which is a separate space far from the operating room. Motion commands of dual instruments are detected, collected, and transmitted to slave side. The slave manipulator is mounted on an operating room (slave side) to replicate the operating actions of physicians. Most importantly, a realistic tactile perception is built through a haptic interface to guarantee the safety of procedure.

A. Master Device

The designed master device is shown in Fig. 2. It is mainly composed of two units: guidewire operating unit (GOU) and

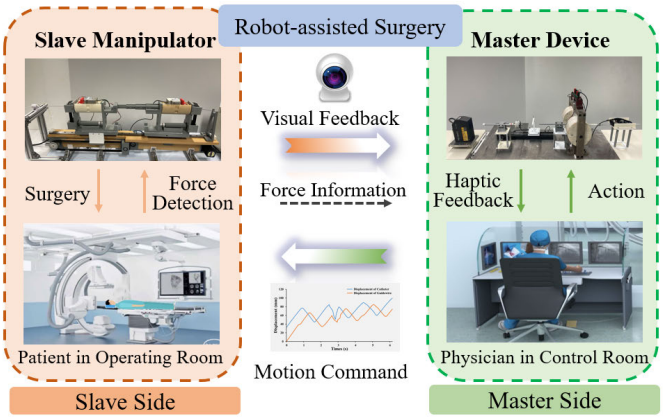

Fig. 1. Conceptual diagram of the proposed robot-assisted VIS.

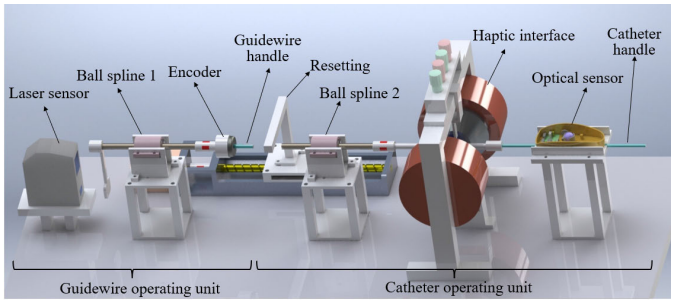

Fig. 2. Designed master device with a couple of operating units and a haptic interface.

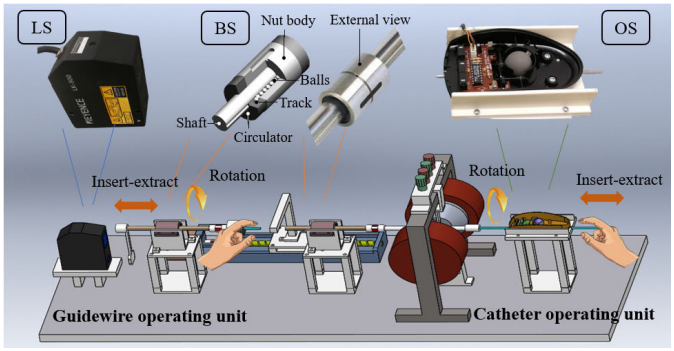

Fig. 3. Core components and available movements for the master device (LS: laser sensor; BS: ball spline; OS: optical sensor).

TABLE I
MAIN SPECIFICATIONS OF THE MASTER DEVICE

Parameter item	Values
Diameter of guidewire handle (rigid rod)	6 mm
Diameter of catheter handle (rigid rod)	3 mm
Diameter of the shaft of ball spline (rigid shaft)	6 mm
Operating distance of GOU (effective movement)	110 mm
Operating distance of COU (effective movement)	100 mm
Movement distance of Resetting	120 mm

catheter operating unit (COU). A haptic interface is mounted on the COU to provide haptic perception. The master device has abilities to capture dual-instrument operation (guidewire and catheter) of interventional surgeons simultaneously and provide significant haptic perception when conducting a surgery. For two operating units, they vary in measurement approaches for both translation and rotation. A laser sensor (LK-500, Keyence Inc., Japan) is utilized to measure the axial movement in the GOU. Meanwhile, an incremental encoder (MES020-2000p, MTL Inc., Japan) is adopted to detect rotational information. In the COU, an integrated optical sensor (Photoelectric mouse M-SBJ96, Fujitsu Inc., Japan) is used to capture the axial motion and radial motion of operations at the same time with an obvious advantage for space-saving and integration measurement. Besides, two ball splines (SLK 006-T2-N5, THK Inc., Taiwan) are installed in operating units to offer stable support, reduce sliding friction, and suppress the jitters of hand operation of surgeons.

To illustrate the better usability of designed master device, Fig. 3 depicts the core components and available movements. The connections and supports of components are realized by 3-D additive manufacturing (ULTRABASE PRO, Anycubic Inc., China). Both two operating handles are cylindrical rigid rods with different diameters, which can mimic a realistic sense of gripping surgical instruments. Two couplings are employed to connect the shaft of ball spline and other components. In addition, a resetting structure is designed to shorten the distance of operation. A stepping motor (VEXTA, ASM46AA, Oriental motor Inc., Japan) with a resolution of 0.36° is applied to drive the screw installed with resetting structure. Benefiting from separate operating handles, it is easy to finish independent operation and simultaneous motion, which offers possibility to deal with multi-instrument vascular interventions. The maximum effective operating distances for COU and GOU are 100 and 110 mm, respectively. Moreover, the elaborative parameters of the master device are listed in Table I.

B. Slave Manipulator

The slave manipulator, previous effort [4] of our group, was presented to insert catheter and guidewire into the blood vessels of patient when physician performs a robot-assisted surgery. Fig. 4 displays the slave manipulator, including catheter control unit and guidewire control unit, corresponding to the two operating units on master side. These two control units are symmetrical designs for inserting and extracting surgical instruments by stepping motors (VEXTA, ASM46AA, Oriental motor Inc., Japan). Synchronous belts are used to finish axial motion for both control units. Two load cells (TU-UJ5N, TEAC Inc., Japan, range: −5 to 5 N) are employed to detect proximal force. The maximum effective distance of moving is 400 mm for two control units and the total length of slave manipulator is 920 mm.

C. Control Console

The elaborate control diagram of developed VIS is realized via serial communication between computer and controller (AT Mega 2560, Arduino.cc, Italy), which is presented in Fig. 5. Controller collected motion data in master device, then transmit captured data to two types of control units in

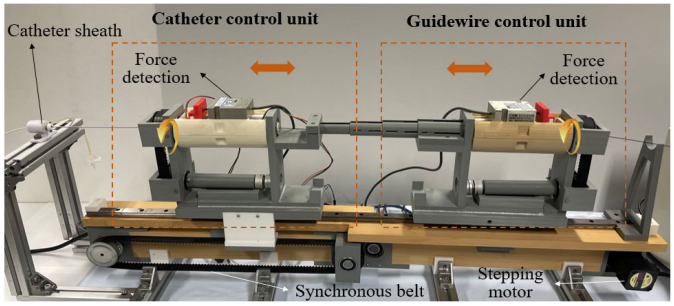

Fig. 4. Slave manipulator for robot-assisted endovascular surgery.

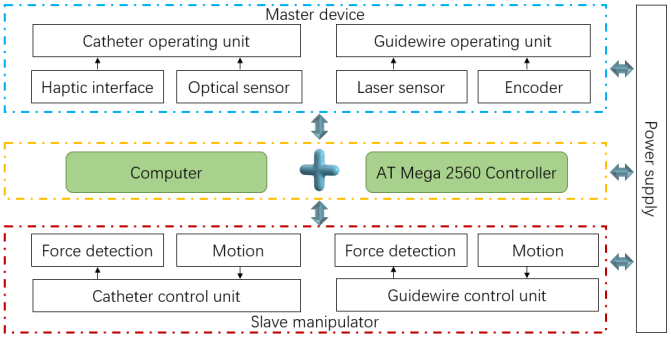

Fig. 5. Control diagram for developed robot-assisted VIS.

slave manipulator. Haptic interface is driven by changing the supplied current (range: 0–3 A).

III. Haptic Interface and Operation Strategy

Haptic feedback and safe operation are significant for robot-assisted VIS to improve the safety for robot-assisted surgeries. Haptic feedback can not only offer a realistic surgical sensing but also sense the insertion position of surgical instrument by different levels of haptic sensation. In this work, we propose a magnetic-actuation-based haptic interface to provide a sense of tactile feedback to surgeons on master device. To show the better usability and ensure a safe environment, the proposed haptic interface, modeling process of core component, working principle of haptic feedback, and a safety operation strategy of VIS are presented for safer operation in this section.

A. Proposed Haptic Interface

To realize a flexible, fast response, and controllable haptic feedback for the robotic system, the haptic interface is designed through a SMAS composed by solid MR block and silicone skin. The solid MR block, which is reprocessed by MR fluid (MRF-122EG, Lord Crop Inc., USA). The silicone (EcoflexTM, 00-20, Smooth-On Inc., USA) is bendable rubber consisted of mixture A and mixture B (mixed in a ratio of 1:1). Two coils (N and S) are produced by 1200 turns of copper wire with the diameter of 1.6 mm. The magnetic field is driven via electric current (by power supply) and delivered by electromagnets. The detailed structure of haptic feedback and relevant characters are shown in Fig. 6. SMAS is assembled by two coils, relevant 3D-printing support, a nonmagnetic shaft, and a curved support [see Fig. 6(b)]. When two coils offer magnetic field, the SMAS will perform a fast response to contact the nonmagnetic shaft, which is depicted in Fig. 6(i). With the growing of flux density for magnetic field, the deformation will embrace a high level to generate haptic resistance, which is drawn in Fig. 6(j). Hence, the core principle of generating haptic feedback for proposed haptic interface is to vary fiction between the nonmagnetic shaft and the SMAS by changing the density of magnetic field.

B. Molding Process of SMAS

The SMAS is molded by the integration of soft material (Silicone) and magnetically controlled material (solid MR block) as a newly soft controllable solution to offer positive resistance for VIS. The thorough molding process is shown in Fig. 7 including three parts: silicone part, solid MR block part, and integration part. In the silicone part, silicone skin is molded through pouring the mixed liquid silicone into designed mold. The rectangular mold is made by 3-D printing technology and can be adjusted for different sizes and depth according to different needs. In solid MR block part, the MR material deposited underneath is utilized to build a rectangular film (MR block) via mixing a cellulose (FLD-1, Xinwang Inc., China). After the steps of pressing and curing, a solid MR block is obtained. Note that the density of MR block is much bigger than the density of liquor silicone. Consequently, a group of rigid needles are neatly put into preprinted holes located in the mold to support the solid MR block after the first molding. At last, the second molding step is adopted to achieve the rest of molding process for silicone skin. Above all, main challenges for molding are to do the reasonable assembly of two materials with different properties. To solve these concerns, mixing the cellulose and placing rigid SMAS include varying the adhesion of MR material and needles, and two times of molding are proposed in this part. The dimensions of designed SMAS are shown in Fig. 8, which is limited according to the actual installation environment of magnetic field [see Fig. 8(c)].

C. Working Principle of Haptic Feedback

The interaction model of haptic feedback between master side and slave side is depicted in Fig. 9. The purpose of force detection is to measure the total force [21] of surgical procedure, which is a proximal force on slave side. The magnetic flux density [22] of a spatial point can be defined as

$$B_a = 2N \frac{\mu_0 i_t R^2}{2\left(\left(R^2 + L_a^2\right)\right)^{1/2}} \tag{1}$$

where $N = 1200$ T represents the number of turns of each coil. $R = 15$ mm is the radius of two irons. L_a is the distance from the spatial point a to the coil, and μ_0 is permeability of vacuum. i_t is the supplied current of electromagnetic coils at the moment t. The working principles of haptic feedback are depicted in Fig. 10. When the SMAS is placed in a uniform magnetic field at tilt angle, the rectangle solid MR block will generate fast action of bending, which is shown in Fig. 10(c). For Fig. 10(d), the magnetic force F_m of the proposed SMAS, which has an angle θ_t with the positive pressure, is a horizontal

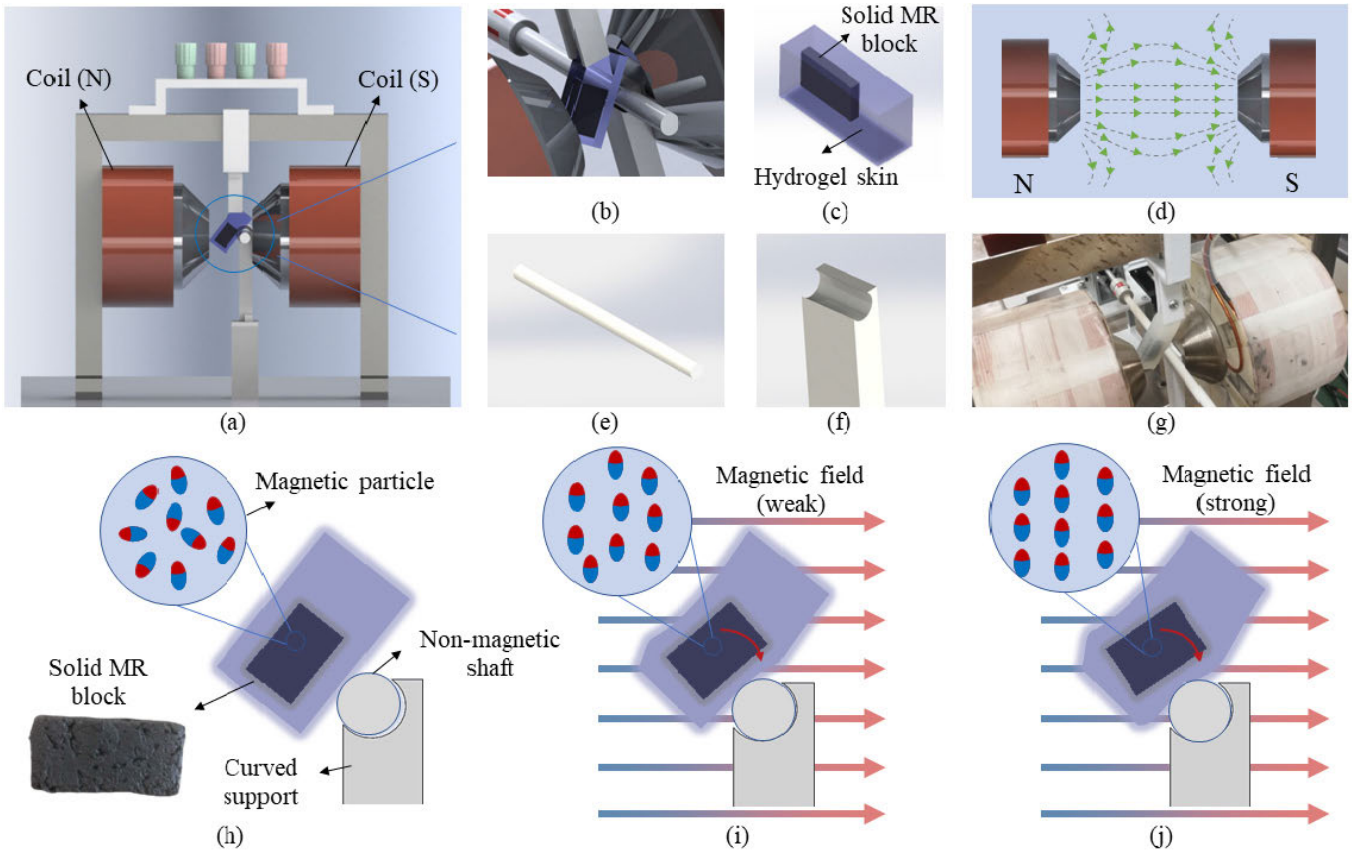

Fig. 6. Proposed haptic interface and relevant characteristics. (a) Main view of haptic interface includes two coils, an SMAS, and relevant 3D-printing support. (b) Core assembly diagram. (c) Schematic of the SMAS. Solid MR block is embedded into silicone skin. (d) Magnetic flux distribution diagram of two coils. (e) Nonmagnetic shaft. (f) Curved support. (g) Real assembly diagram of haptic interface. (h) Expression of the SMAS without magnetic field. (i) Expression of the SMAS within weak magnetic field. (j) Expression of the SMAS within strong magnetic field.

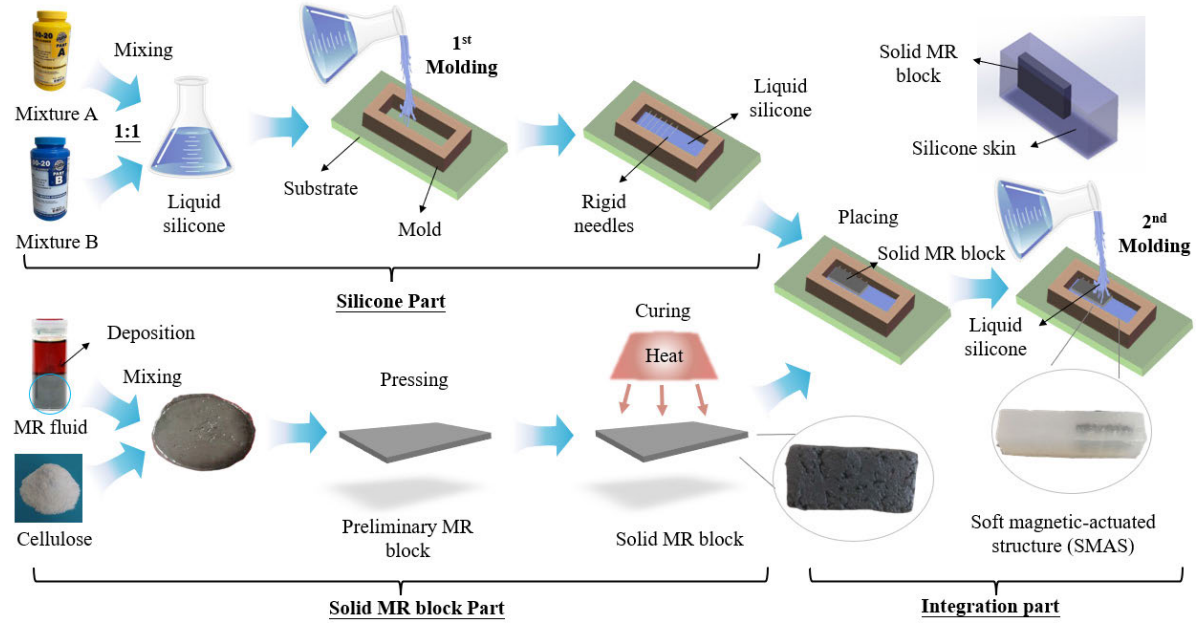

Fig. 7. Molding process of the designed SMAS. There are three parts in the procedure including silicone part, solid MR block part, and integration part. Additionally, two times of molding are displayed to fabricate the solid MR block and the silicone skin for SMAS.

active force due to the interaction of magnetic field and solid MR block. The positive pressure F_p is a force go through the core contact points A_1 and A_2, which can be expressed as

$$F_p = \cos\theta_t (F_m - F_r), \quad (F_m > 0, F_r > 0, F_m > F_r) \quad (2)$$

where F_p represents the positive pressure from the SMAS to the nonmagnetic shaft. F_r is the deformation resistance of the silicone skin. θ_t is the angle between the magnetic force F_m of SMAS and the positive pressure F_p, which is a variable parameter with the moment t and the magnetic flux density B_a.

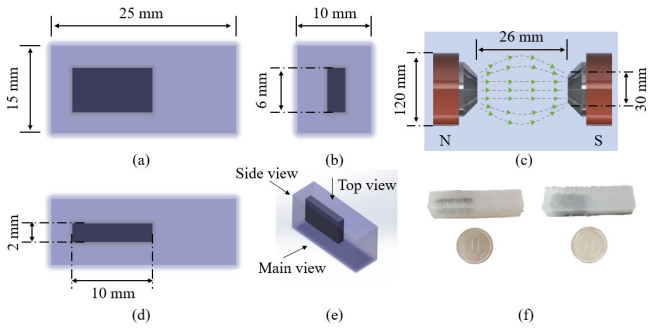

Fig. 8. Designed SMAS based on soft silicone skin and solid MR block. (a) Main view. (b) Side view. (c) Installation environment of two coils. (d) Top view. (e) Schematic of the SMAS. (f) Real molded SMAS.

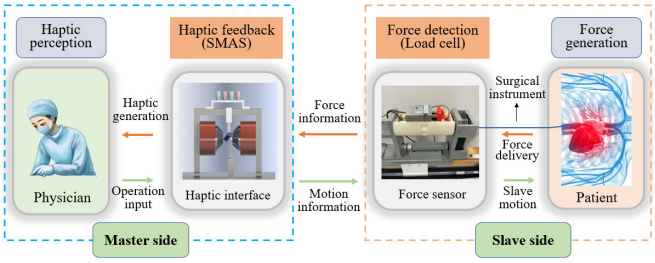

Fig. 9. Interaction model of haptic feedback on the robot-assisted vascular interventional system.

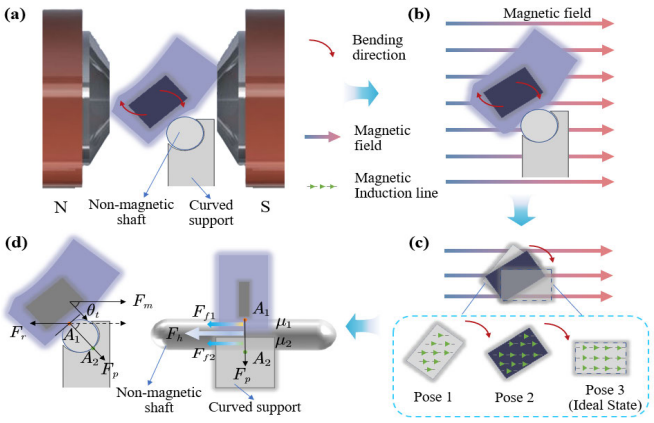

Fig. 10. Working principles of haptic feedback. (a) Installation diagram. (b) Actions of SMAS under magnetic field. (c) Distribution of magnetic inductions line for solid MR block in different pose. (d) Principles of haptic feedback in main view and the cross-sectional view.

On the right side of Fig. 10(d), the cross-sectional view from the positive pressure F_p is depicted. Operators can sense the haptic feedback F_h when operate the nonmagnetic shaft, which is a total friction in the haptic interface. The force relationship can be described as

$$\begin{aligned} F_h &= F_{f1} + F_{f2} \\ F_{f1} &= \mu_1 F_p, \quad F_{f2} = \mu_2 F_p \end{aligned} \tag{3}$$

where F_h represents the perception of haptic feedback to operator. F_{f1} is the friction from the contact surface of SMAS and nonmagnetic shaft. F_{f2} is the friction from the contact surface of curved support and nonmagnetic shaft. Notably, both of the contact areas for F_{f1} and F_{f2} are curved surface, which are able to offer stable and feasible friction to the nonmagnetic shaft. μ_1 means the friction coefficient between the bended SMAS and the nonmagnetic shaft. μ_2 means the friction coefficient between the nonmagnetic shaft and the curved support. Calculating (3), haptic feedback is obtained by

$$F_h = \mu_1 F_p + \mu_2 F_p, \quad (\mu_1 > 0, \mu_2 > 0). \tag{4}$$

According to the molecular-mechanical friction theory, the actual friction coefficients μ_1 and μ_2 are relative with the contact area of two surfaces. The expression can be written as

$$\mu_1 = \alpha_1 A_{r(1)}, \quad \mu_2 = \alpha_2 A_{r(2)} \tag{5}$$

where α_1 and α_2 are the two parameters related to the molecular properties of different contact surface. $A_{r(1)}$ and $A_{r(2)}$ represent the contact areas of two contact surfaces, respectively. These two contact areas can be expressed as

$$A_{r(i)} = \left(\frac{A_{ci} \cdot \gamma \cdot F_{\mathrm{Ni}}^2}{C_i E^2 R_a} \right)^{\frac{1}{3}}, \quad (i = 1, 2) \tag{6}$$

where A_{ci} represents the real contact areas, γ is the roughness radius, F_{Ni} means normal load on surface, E is the material elastic modulus, R_a represents the roughness mean square error, and C_i is the constant value. Substituting (5) and (6) into (4) results in

$$F_h = \alpha_1 F_p \left(\frac{A_{c1} \cdot \gamma \cdot F_{\mathrm{N1}}^2}{C_1 E^2 R_a} \right)^{\frac{1}{3}} + \alpha_2 F_p \left(\frac{A_{c2} \cdot \gamma \cdot F_{\mathrm{N2}}^2}{C_2 E^2 R_a} \right)^{\frac{1}{3}}. \tag{7}$$

When F_p is controlled appropriately, various levels of haptic feedback can be precepted by physicians when operate master device. Moreover, the soft magnetic-actuation-based haptic interface also has potential ability to provide rotational haptic feedback in the future.

D. Safety Operation Strategy

An operation strategy is proposed to ensure a safer robot-assisted surgical environment, as shown in Fig. 11. The proximal force F_S is captured by load cell. Three kinds of operations named dangerous operation, potentially unsafe operation, and safe operation are classified by the value of F_S. Two thresholds $F_A = 1.0$ N and $F_B = 0.342$ N (thresholds refer to [3]) are utilized to divide three operations. The presented operating strategy is described as follows.

1) *Dangerous Operation:* When the proximal force is over 1.0 N, compulsory protection and reinforced haptic feedback are used to extract the surgical instrument quickly and remind the operator to conduct safe operation timely. E_0 is a constant reduction value (20 pulses) for the signal of linear motion X_m (a number of pulses) collected in master device. The corrected motion data X_m'' will be delivered to the master manipulator for linear motion. Moreover, haptic feedback is reinforced to offer a magnified perception by varying the value of supplied current βi (β is a positive parameter greater than 1).
2) *Potentially Unsafe Operation:* When the detected force is over 0.342 N, an interaction control is proposed to decrease the motion data by the following equation:

$$X_m' = X_m - \gamma(F_S - F_B) \tag{8}$$

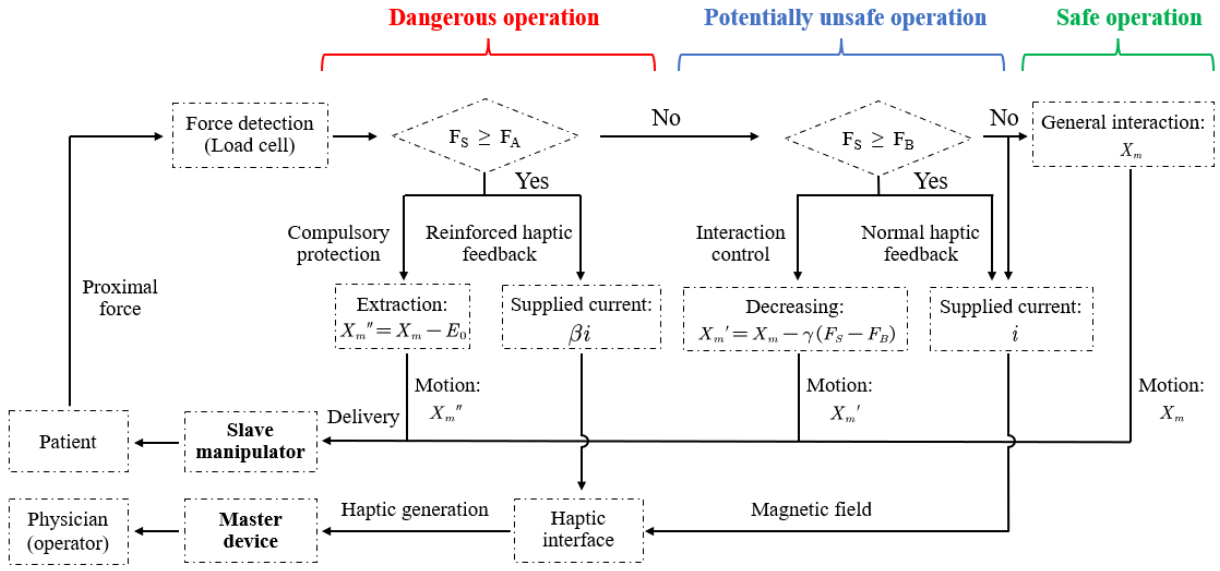

Fig. 11. Flowchart of safety operation strategy for the robot-assisted vascular interventional system.

where X'_m is the decreased motion signal. γ is the adjustment factor, which can be determined by patient's surgical environment. F_S is the detected proximal force on slave side. After the procedure of decreasing, slave manipulator will obtain the motion X'_m to generate a tiny displacement for safety operation.

3) *Safe Operation:* When the proximal force is less than 0.342 N, it is considered as a safe operation. In this case, normal haptic feedback and general interaction are employed between master device and slave manipulator. The motion data X_m captured on master side will be transmitted to slave manipulator directly.

The safety operation strategy mainly occurs on master side to produce different levels of haptic feedback and remind the operator about the actual surgical conditions (safe or not).

Benefiting this operation strategy, physician can complete a robot-assisted surgery with low risk of operation.

IV. Experiments and Results

In this section, four types of experiments were conducted to verify relevant feasibility and performance of this work, including characteristics testing, calibration experiment of haptic interface, tracking performance of master–slave side, and operation performance of the robot-assisted VIS.

A. Characteristics Testing

In order to choose a better size of SMAS and explore the advantages of the proposed soft solution, relevant tests are conducted for silicone skin and SMAS. Characteristics' experiments for designed silicone skin insist of stretchability, compressibility, and capacity of shape memory, which are significant for deformation properties of soft material. For the properties of designed SMAS, three kinds of tests are proposed to demonstrate the recovery performance via front bending, side bending, and magnetic field.

Characteristics' tests for silicone skins are shown in Fig. 12 and include tests for two types of silicone skins with different

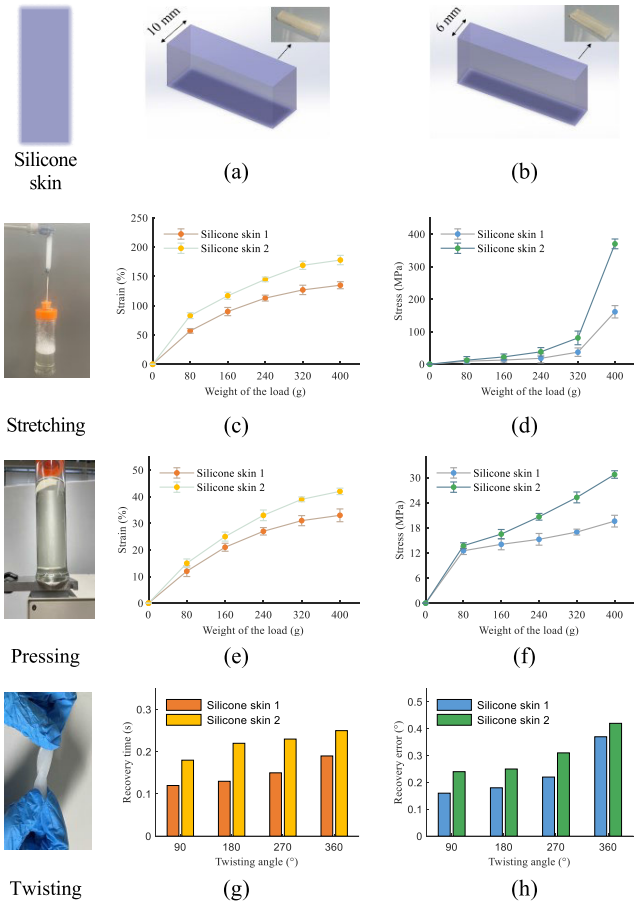

Fig. 12. Characteristics tests for silicone skins. (a) Silicone skin 1. (b) Silicone skin 2. (c) Results of strain. (d) Results of stress. (e) Results of strain. (f) Results of stress. (g) Results of recovery time with distinct twisting angle. (h) Results of recovery error within various twisting angles.

thicknesses (10 and 6 mm). The tests for stretching and pressing are conducted by varying the weight of load, which is measured by a metrology balance (GX-400, A&D Inc., Japan)

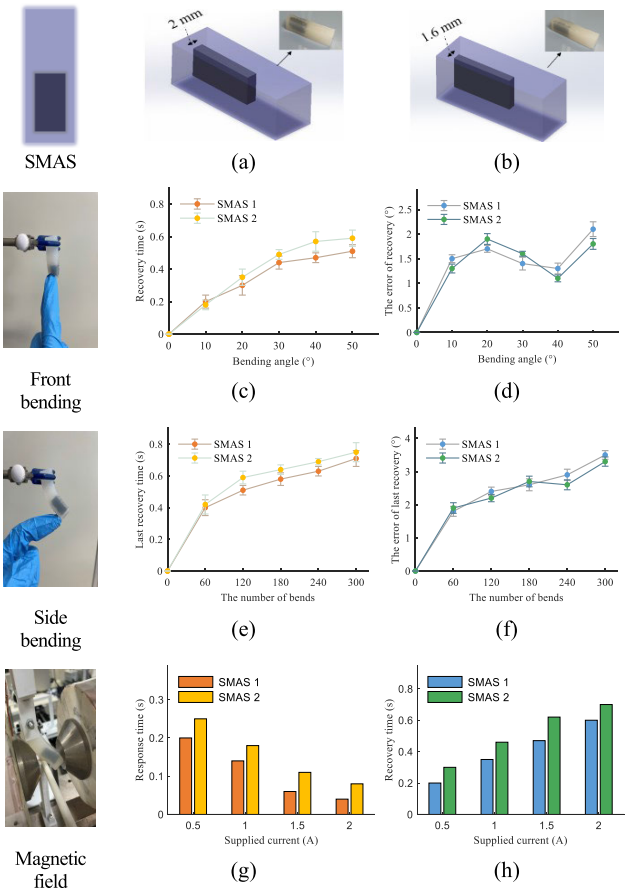

Fig. 13. Characteristics tests for SMAS. (a) SMAS 1. (b) SMAS 2. (c) Results of recovery time. (d) Results of error. (e) Results of last recovery time. (f) Results of error. (g) Results of response time under distinct supplied current. (h) Results of recovery time within various supplied currents.

with a range from 0.02 to 410 g. The general definition of Young's modulus E_{hydrogel} is described as

$$E_{\text{hydrogel}} = \frac{\sigma}{\varepsilon} = \frac{\left(F_{\text{positive}}/A_{\text{vertical}}\right)}{(\Delta L/L_0)} \tag{9}$$

where σ and ε are the uniaxial stress and strain, respectively. F_{positive} is the positive compression or extension force, which is equal to the weight of the load. A_{vertical} represents the cross-sectional area. ΔL and L_0 are the variation of length and the original length of silicones, respectively. It is easy to see that silicone skins embrace significant advantages for stretching [tests of strain and stress for different loads, see Fig. 12(c) and (d)], pressing [tests of strain and stress for different loads, see Fig. 12(e) and (f)], and fast recovery (less than 0.3 s) after twisting. Particularly, silicone skin 1 (with a thickness of 10 mm) shows better recovery performance [see Fig. 12(g) and (h)] compared to another skin. Consequently, the thickness of 10 mm is selected to be the parameter for molded SMAS.

Testing characteristics for SMAS are displayed in Fig. 13. Although solid MR blocks with different thicknesses (2 and 1.6 mm) were embedded into two SMASs, recovery time has no obvious drop for both front bending and side bending [see Fig. 13(c)–(f)]. The maximum testing number is set to

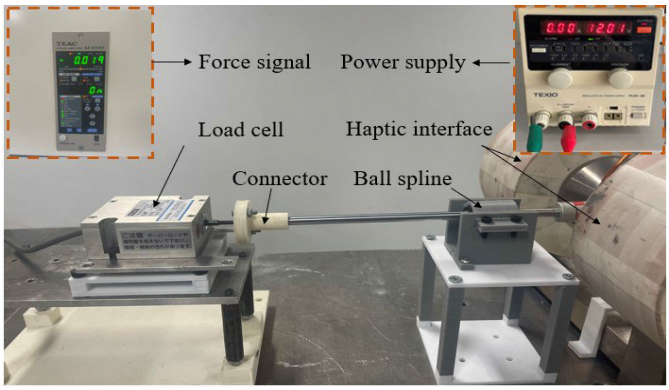

Fig. 14. Experimental setup for the calibration of haptic interface.

300 for the side bending with a fixed growth step of 60. In addition, both SMASs are installed into the paired coils to test the characteristics of response and recovery. The magnetic field is generated and changed by a power supply. Analyzing Fig. 13(g) and (h), the proposed SMAS has fast response time (less than 0.3 s) and good recovery time (average values are 0.41 and 0.52 s, respectively) when supplying a magnetic field. Notably, the recovery time of Fig. 13(h) is larger than Fig. 13(g) due to the nonlinear hysteresis properties of magnetic materials. Based on this test, designed SMAS as a new magnetically controlled solution has abilities to offer a fast and repeatable haptic feedback for rapid tactile perception in robot-assisted vascular surgery, which has significant value to improve operation safety for physicians.

B. Calibration Experiment of Haptic Interface

1) Experimental Setup: The experimental setup for Experiment B is shown in Fig. 14. The load cell was mounted on the left end of ball spline by a connector. Force signal was displayed on the strain amplifier with a minimum sensitivity of ±0.01% F.S (SA-570ST, TEAC Inc., Japan). A power supply (range: 0–3 A) was used to offer a variable magnetic field for haptic interface. We collected the value of magnetic flux density measured by a Tesla Meter (TM-701, KANETEC Inc., Japan) via changing supplied current at a fixed incremental step (0.1 A). Considering the hysteresis property of MR material, two kinds of collections for magnetic flux density were carried out with SMAS and without SMAS. Second, five types of designed SMAS with different thicknesses (1.6, 1.8, 2.0, 2.2, and 2.4 mm) of solid MR block were used to complete the calibration experiment between the supplied current and the force of haptic feedback. When the sliding of SMAS occurs, the strain amplifier can capture the force signal of resistance timely.

2) Experimental Results: The magnetic flux density of haptic interface with SMAS and without SMAS was shown in Fig. 15. The value of magnetic flux density gradually rises as the growth of supplied current. An interesting thing is that red line (with SMAS) is higher than blue line (without SMAS) due to the hysteresis characteristics.

Considering when the supplied current is over 2.5 A, the magnetic field (value is close to 200 mT) is not stable and easy to control [23] even along with greater operating experimental

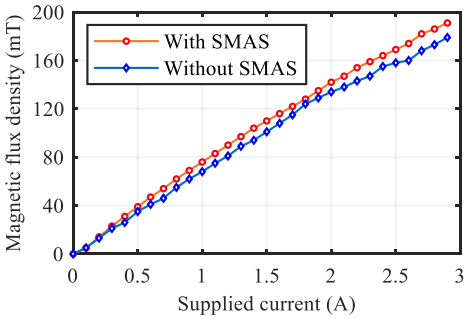

Fig. 15. Relationship between the supplied current and the magnetic flux density.

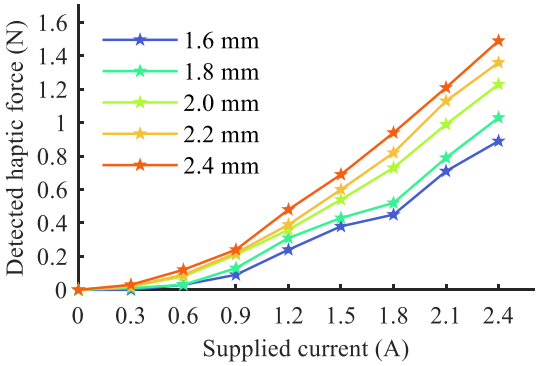

Fig. 16. Relationship between the supplied current and detected haptic force within different thicknesses of solid MR block.

error. Hence, the value of experimental current for SMAS is limited below 2.5 A. The relationship between the supplied current and detected haptic force within different SMSAs is shown in Fig. 16. When the current is less than 0.9 A, haptic force embraces a slow increasing. The reason is probably the particular co-interaction between the bending property of silicone skin (soft material) and the MR solid block (magnetic material). The maximum haptic force is 1.49 N, and the minimum haptic force of this robotic system is 0.01 N (human hands do not feel it, detected by load cell). The minimum identifiable force is 0.21 N (detected by the experiments of hands) in calibration experiment. Above all, the proposed haptic feedback based on the SMAS is a feasible and flexible solution of haptic feedback for robotic system.

C. Tracking Performance of Master–Slave Side

1) Experimental Setup: For the master–slave operating VIS, tracking performance [4] is significant for both manipulation units (catheter unit and guidewire unit). Linear operation and rotary operation are conducted in this part. A laser sensor (LK-080, Keyence Inc., Japan) with a precision of 3 μm/mV is used to capture the displacement of manipulation units on the slave side. We set various speeds (2, 4, 6, 8, and 10 mm/s) for linear operation to arrive at a target at the displacement of 40 mm. For rotation, an encoder (CB-1000D, Line Seiki Company Ltd., Japan), the precision is 0.09°/pulse, is employed to collect the rotation information of manipulation units. The operating angles are set to 60°, 120°, 180°, 270°, and 360° on master side. Each trial is set to ten times in this part.

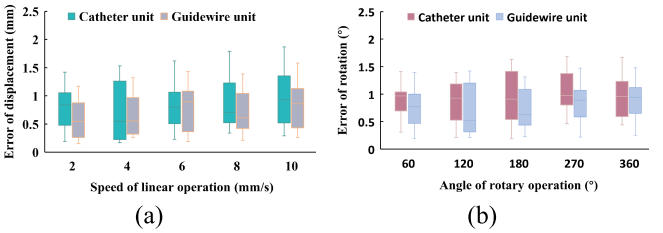

Fig. 17. Tracking performance of master–slave side. (a) Error of linear operation within distinct speeds. (b) Error of rotary operation within distinct angles.

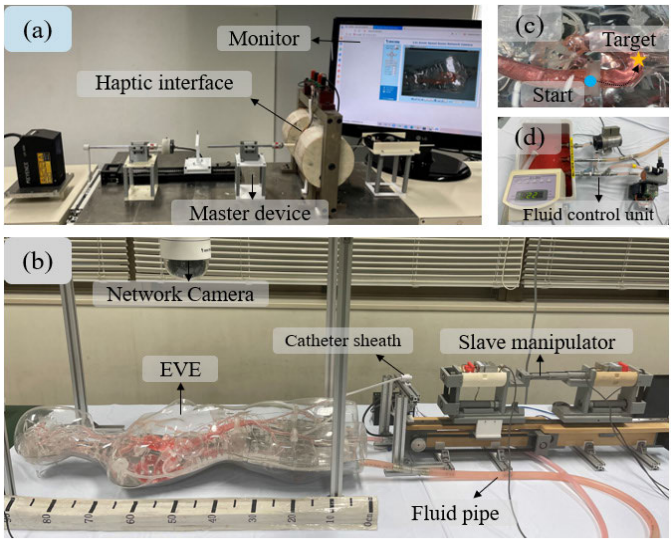

Fig. 18. Experimental setup of vitro experiments. (a) Slave side. (b) Master side. (c) Surgical task. (d) Fluid control unit.

2) Experimental Results: The experimental results are shown in Fig. 17. The error of displacement for linear operation and the error of angle for rotary operation are drawn in Fig. 17(a) and (b), respectively. The maximum linear error of catheter unit is 1.87 mm, and the maximum linear error of guidewire unit is 1.58 mm. Furthermore, the maximum rotation error of catheter unit is 1.69°, and the maximum rotation error of guidewire unit is 1.48°. Rotation is used to correct the direction when insert the surgical instruments, and the risk of damaging the blood vessel is small during operation [4].

D. Operating Performance in Vitro Experiments

1) Experimental Setup: Aiming to validate the operation performance of the proposed robot-assisted VIS, vitro experiments are conducted to complete the evaluation process. An endo vascular evaluator (EVE, Fain-Biomedical Inc., Japan) was used to insert/extract catheter and guidewire, which can simulate actual surgical environment of patient. The fluid control unit insists of a bellows pump (KB-4N, Iwaki Ltd., Japan), a magnet pump (PMD-121B7B1, Sanso Ltd., Japan), and a Thermal Robo (TR-1AR, AS ONE Corporation, Japan). The objective of fluid control unit is to achieve safe and real control of the pumped fluid at appropriate pressure and temperature (fluid pressure is 1.5 mmHg and experimental temperature is 25.3 °C). The experimental setup is shown in Fig. 18. From the start position to the target position, there

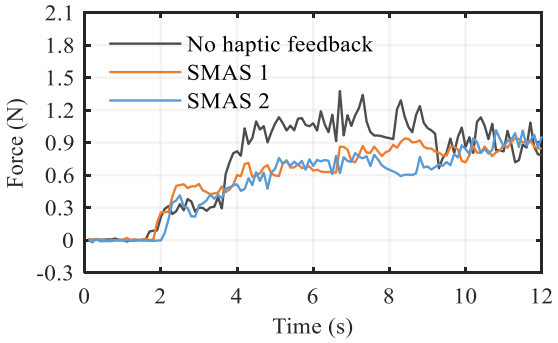

Fig. 19. Example of force comparison for catheter unit on the slave side during different operations.

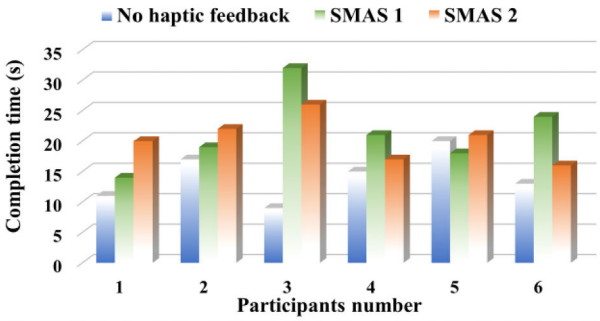

Fig. 20. Comparison for completion time under three operations.

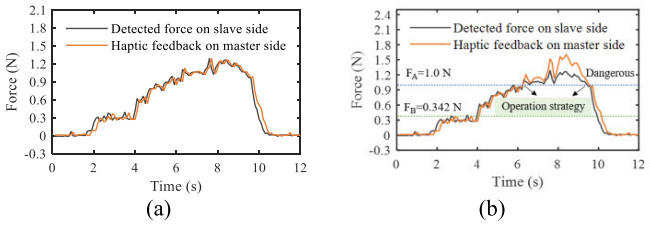

Fig. 21. Relationship between the detected force on the slave side and the haptic feedback on the master side. (a) Comparison without operation strategy. (b) Comparison with operation strategy.

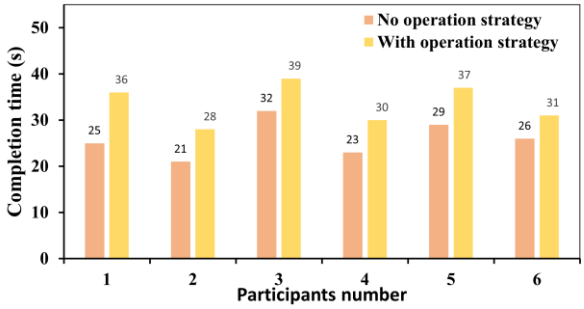

Fig. 22. Comparison for completion time with the safety operation strategy or not.

are a smooth part of aorta and a part of arterial arch. A long guidewire is with the length of soft tip of 3 cm. The catheter employed is a 4 Fr catheter (1 Fr $\approx$ 0.333 mm Terumo Company, Japan). Six participants were invited to conduct the robot-assisted surgery by manipulating the catheter control unit (haptic feedback is mounted on COU). The performance evaluation is consisted of two metrics.

1) The detected force on the slave side without haptic feedback and with two kinds of soft SMAS (SMAS 1 and SMAS 2, see Fig. 13). Additionally, the completion time was collected under three cases as well.
2) The relationship between the detected force on the slave side and the haptic feedback on the master side using the safety operation strategy or not. Besides, the completion time of tasks was also recorded.

2) Experimental Results: The contrastive experimental results are shown in Fig. 19. The force of catheter was collected when participants operate the robotic system to reach the target. The maximal force for the case of no haptic feedback is 1.38 N. The maximal force for the case with SMAS 1 is 1.01 N. The maximal force for the case with SMAS 2 is 0.94 N. The recorded completion times of six participants for three cases are shown in Fig. 20. The maximum values of completion time are 20, 32, and 26 s, respectively. Correspondingly, the minimum completion times are 9, 14, and 16 s for three types of operations.

Moreover, the relationship between the detected force on the slave side (black line) and haptic feedback on the mater side (orange line) is shown in Fig. 21. The comparison results with the safety operation strategy (is set to 1.3 in this work) are drawn in Fig. 21(b). In addition, the collected completion time for participant is drawn in Fig. 22. The maximal completion time with safety operation strategy is 39 s. The maximal completion time without safety operation strategy is 32 s.

V. Discussion

For the objective of accurate reproduction of natural surgical skills and operational needs for separate master–slave design [19], a robot-assisted VIS with soft magnetic-actuation-based haptic interface was proposed as a novel solution of haptic sensing based on soft material and magnetic material. Feasibility study for haptic feedback and an operation strategy are proposed for the robot-assisted VIS.

From the characteristics testing (see Fig. 12), the silicone skin is well performed in stretchability, compression, and bendability. The proposed soft haptic feedback structure has abilities to achieve deformation many times, fast recovery when bending occurs, and good mechanical performance under magnetic field (see Fig. 13). In Section IV, the relationship between supplied current and detected haptic force (see Fig. 16) displays the situation of haptic sensation (minimum force is 0.01 N). From tracking performance (see Fig. 17), the maximum linear error of manipulation units is 1.87 mm, which satisfy the requirements of operation (when the error is less than 2 mm, operation is safe [8]). Moreover, the operation performance of EVE experiments exhibits that the maximum force has a decreasing when operation within haptic feedback (see Fig. 18). The operation with haptic feedback costs more time than the case without haptic feedback (see Fig. 20). An interesting thing is that completion time under safety operation strategy is a bit longer than normal operation (see Fig. 22), which mainly contribute to that reinforced haptic feedback (by amplifying the applied current, see Fig. 21)

TABLE II
COMPARISON OF HAPTIC FEEDBACK WITH OTHER EXISTING METHODS

Relevant efforts	Implementations	Sensing range	Minimum identifiable force
Yang et al. [11]	Linear motor	0N-3.5N	Not mentioned
Zhou et al. [18]	Springs	0.247N-4.5N	0.247 N
Bao et al. [24]	TouchTM (Commercial product)	0N-3N (roughly)	Not mentioned
This effort	Soft magnetic-actuated haptic Interface	**0.01-1.49N**	**0.01 N**

offers a warning for safety operation. This issue is possible to be improved by pretraining for operators and optimizing data transmission technology. Accordingly, the developed VIS is favorable and feasible for robot-assisted surgery.

The comparison of haptic feedback with other existing methods is shown in Table II, and the proposed robotic system demonstrates advantages for the performance of haptic feedback. Our effort displays a more flexible and more accurate value of haptic force (0.01–1.49 N) compared with an isomorphic interactive device (0–3.5 N [11]). A surgeon's habits-based master manipulator [18] was designed with minimum identifiable force of 0.247 N as a single-instrument manipulator (the minimum identifiable force is 0.21 N in our work). TouchTM [24], commercial haptic device, was employed to collect movements and generate haptic feedback with a force range of 0–3 N. From Table II, the proposed haptic interface is able to offer more accurate and controllable haptic feedback for robot-assisted vascular intervention.

Notably, not only silicone skin (soft material) is green and compatible, but also the solid MR block (magnetic material) is compatible and controllable. Compared to permanent magnets, the proposed SMAS has better compatibility and controllability for haptic as a soft solution. Moreover, the proposed system offers two alternative operating units on the master side (see Fig. 2), which can provide different solutions for complicated surgery. Furthermore, the presented safety operating strategy gives a safer surgical environment when conduct robot-assisted surgery (see Fig. 20), which make the interaction between surgeons and patients more comfortable and stable.

In addition, there are a few limitations for this study including the fabrication precision of SMAS, loss actual insertion experiments for animals and humans, and a little bit delay might exist. Although relative works for these limitations are still in an immature stage, the proposed haptic interface inspires a new research topic on a reasonable combination for the field of soft material and filed of magnetic-actuation-based material for haptic feedback. Moreover, this developed VIS will be more accurate, practical, and applicable by integrating advanced methods, including a simplified linear model [25], model-free generative adversarial imitation learning [26], catheter design with special functions [27], and even adding evaluation of operational behavior [28].

VI. CONCLUSION

In this effort, a dual-instrument operating VIS was proposed to manipulate both catheter and guidewire for multi-instrument surgical procedures. Particularly, a newly soft solution, magnetic-actuation-based haptic interface, was designed to generate the adjustable sensation of haptic feedback for surgeons. Furthermore, a safety operation strategy based on the proposed haptic interface was presented to ensure a safer surgical environment. Through four types of experiments, the feasibility of soft magnetic-actuation-based haptic feedback, tracking performance, and operating performance of developed robot-assisted VIS has been evaluated. The experimental results illustrate that the proposed robotic system has advantages for movements with a maximum linear error of 1.87 mm, the feasibility of haptic feedback (range: 0.01–1.49 N), and safety operation based on the proposed strategy. This study also has potential inspirations for human–machine interaction, research on soft controllable materials, and enhancement of safety operation for other robotics engineering.

The future work will pay attention to further evaluation and application of soft magnetic-actuation-based haptic interface, even verify the proposed robot-assisted VIS in vivo experiments.

REFERENCES

[1] P. Shi et al., "Design and evaluation of a haptic robot-assisted catheter operating system with collision protection function," *IEEE Sensors J.*, vol. 21, no. 18, pp. 20807–20816, Sep. 2021.

[2] Y. Yan et al., "Machine learning-based surgical state perception and collaborative control for a vascular interventional robot," *IEEE Sensors J.*, vol. 22, no. 7, pp. 7106–7118, Apr. 2022.

[3] X. Jin, S. Guo, J. Guo, P. Shi, M. Kawanishi, and H. Hirata, "Active suppression method of dangerous behaviors for robot-assisted vascular interventional surgery," *IEEE Trans. Instrum. Meas.*, vol. 71, pp. 1–9, 2022, doi: 10.1109/TIM.2022.3170997.

[4] X. Li, S. Guo, P. Shi, X. Jin, M. Kawanishi, and K. Suzuki, "A bimodal detection-based tremor suppression system for vascular interventional surgery robots," *IEEE Trans. Instrum. Meas.*, vol. 71, pp. 1–12, 2022, doi: 10.1109/TIM.2022.3216367.

[5] X. Jin, S. Guo, J. Guo, P. Shi, T. Tamiya, and H. Hirata, "Development of a tactile sensing robot-assisted system for vascular interventional surgery," *IEEE Sensors J.*, vol. 21, no. 10, pp. 12284–12294, May 2021.

[6] M. E. M. K. Abdelaziz et al., "Toward a versatile robotic platform for fluoroscopy and MRI-guided endovascular interventions: A preclinical study," in *Proc. IEEE/RSJ Int. Conf. Intell. Robots Syst. (IROS)*, Nov. 2019, pp. 5411–5418.

[7] X. Li, S. Guo, P. Shi, and X. Jin, "A novel tremor suppression method for endovascular interventional robotic systems," in *Proc. IEEE Int. Conf. Mechatronics Autom. (ICMA)*, Aug. 2021, pp. 1050–1054.

[8] L. Zhang et al., "Design and performance evaluation of collision protection-based safety operation for a haptic robot-assisted catheter operating system," *Biomed. Microdevices*, vol. 20, no. 2, pp. 1–14, 2018, doi: 10.1007/S10544-018-0266-8.

[9] X. Yin, S. Guo, N. Xiao, T. Tamiya, H. Hirata, and H. Ishihara, "Safety operation consciousness realization of a MR fluids-based novel haptic interface for teleoperated catheter minimally invasive neurosurgery," *IEEE/ASME Trans. Mechatronics*, vol. 21, no. 2, pp. 1043–1054, Apr. 2016.

[10] X. Yin, C. Wu, S. Wen, and J. Zhang, "Smart design of Z-Width expanded thumb haptic interface using magnetorheological fluids," *IEEE Trans. Instrum. Meas.*, vol. 70, pp. 1–11, 2021, doi: 10.1109/TIM.2021.3112231.

[11] C. Yang, S. Guo, and X. Bao, "An isomorphic interactive device for the interventional surgical robot after in vivo study," *Micromachines*, vol. 13, no. 1, p. 111, Jan. 2022.

[12] X. Bao, S. Guo, N. Xiao, Y. Li, C. Yang, and Y. Jiang, "A cooperation of catheters and guidewires-based novel remote-controlled vascular interventional robot," *Biomed. Microdevices*, vol. 20, no. 1, pp. 1–19, Mar. 2018.
[13] X. Bao et al., "Operation evaluation in-human of a novel remote-controlled vascular interventional robot," *Biomed. Microdevices*, vol. 20, no. 2, p. 34, Apr. 2018.
[14] D. Kundrat et al., "An MR-safe endovascular robotic platform: Design, control, and ex-vivo evaluation," *IEEE Trans. Biomed. Eng.*, vol. 68, no. 10, pp. 3110–3121, Oct. 2021.
[15] K. Wang et al., "Endovascular intervention robot with multi-manipulators for surgical procedures: Dexterity, adaptability and practicability," *Robot. Comput.-Intergr. Manuf.*, vol. 56, pp. 75–84, Apr. 2019.
[16] T. Chen et al., "Novel, flexible, and ultrathin pressure feedback sensor for miniaturized intraventricular neurosurgery robotic tools," *IEEE Trans. Ind. Electron.*, vol. 68, no. 5, pp. 4415–4425, May 2021.
[17] A. Hooshiar, A. Sayadi, J. Dargahi, and S. Najarian, "Integral-free spatial orientation estimation method and wearable rotation measurement device for robot-assisted catheter intervention," *IEEE/ASME Trans. Mechatronics*, vol. 27, no. 2, pp. 766–776, Apr. 2022.
[18] W. Zhou, S. Guo, J. Guo, F. Meng, Z. Chen, and C. Lyu, "A surgeon's habits-based novel master manipulator for the vascular interventional surgical master-slave robotic system," *IEEE Sensors J.*, vol. 22, no. 10, pp. 9922–9931, May 2022.
[19] S. Guo et al., "A novel robot-assisted endovascular catheterization system with haptic force feedback," *IEEE Trans. Robot.*, vol. 35, no. 3, pp. 685–696, Jun. 2019.
[20] G. Dagnino, J. Liu, M. E. M. K. Abdelaziz, W. Chi, C. Riga, and G.-Z. Yang, "Haptic feedback and dynamic active constraints for robot-assisted endovascular catheterization," in *Proc. IEEE/RSJ Int. Conf. Intell. Robots Syst. (IROS)*, Oct. 2018, pp. 1770–1775.
[21] X. Jin et al., "Total force analysis and safety enhancing for operating both guidewire and catheter in endovascular surgery," *IEEE Sensors J.*, vol. 21, no. 20, pp. 22499–22509, Oct. 2021.
[22] Z. Wang, S. Guo, J. Guo, Q. Fu, L. Zheng, and T. Tamiya, "Selective motion control of a novel magnetic-driven minirobot with targeted drug sustained-release function," *IEEE/ASME Trans. Mechatronics.*, vol. 27, no. 1, pp. 336–347, Feb. 2022.
[23] X. Li, S. Guo, P. Shi, X. Jin, and M. Kawanishi, "An endovascular catheterization robotic system using collaborative operation with magnetically controlled haptic force feedback," *Micromachines*, vol. 13, no. 4, p. 505, Mar. 2022.
[24] X. Bao et al., "Multilevel operation strategy of a vascular interventional robot system for surgical safety in teleoperation," *IEEE Trans. Robot.*, vol. 38, no. 4, pp. 2238–2250, Aug. 2022.
[25] D.-H. Lee, Y.-H. Kim, J. Collins, A. Kapoor, D.-S. Kwon, and T. Mansi, "Non-linear hysteresis compensation of a tendon-sheath-driven robotic manipulator using motor current," *IEEE Robot. Autom. Lett.*, vol. 6, no. 2, pp. 1224–1231, Apr. 2021.
[26] W. Chi et al., "Collaborative robot-assisted endovascular catheterization with generative adversarial imitation learning," in *Proc. IEEE Int. Conf. Robot. Autom. (ICRA)*, May 2020, pp. 2414–2420.
[27] S. Kang and D. Y. Lee, "Hydraulically steerable micro guidewire capable of distal sharp steering," *IEEE Trans. Biomed. Eng.*, vol. 68, no. 2, pp. 728–735, Feb. 2021.
[28] J. Sikorski, C. M. Heunis, F. Franco, and S. Misra, "The ARMM system: An optimized mobile electromagnetic coil for non-linear actuation of flexible surgical instruments," *IEEE Trans. Magn.*, vol. 55, no. 9, pp. 1–9, Sep. 2019.

Xinming Li (Graduate Student Member, IEEE) is currently pursuing the Ph.D. degree in intelligent mechanical systems engineering with the Graduate School of Engineering, Kagawa University, Takamatsu, Japan.

He has authored over five refereed journals and conference papers. His research includes robotic catheter systems, safety operation, and haptic feedback.

Shuxiang Guo (Fellow, IEEE) is currently a Chair Professor with the Department of Electronic and Electrical Engineering, Southern University of Science and Technology, Shenzhen, China. He is also a Chair Professor with the Key Laboratory of Convergence System and Healthcare Technology Medical Engineering, Beijing Institute of Technology, Beijing, China. His research interests include medical robot systems and microcatheter systems.

Prof. Guo has a fellowship of The Engineering Academy of Japan.

Keisuke Suzuki is currently a Professor with the Graduate School of Engineering, Kagawa University, Takamatsu, Japan.

Prof. Suzuki is a Fellow of JSAE. He is also the Chairperson of the Advanced Simulator Study Group organized by JSME.

Peng Shi (Member, IEEE) received the Ph.D. degree in intelligent mechanical systems engineering from Kagawa University, Takamatsu, Japan, in 2022.

He has authored over six refereed journals and conference papers. His research interests include catheter robotic systems, haptic feedback, and virtual reality systems.

Xiaoliang Jin (Member, IEEE) received the Ph.D. degree in intelligent mechanical systems engineering from Kagawa University, Takamatsu, Japan, in 2022.

He has authored over eight refereed journal and conference papers. His research interests include catheter robotic systems, force control, and haptic feedback.